

# Viscoelastic properties of linear associating poly(n-butyl acrylate) chains

L. G. D. Hawke



*Bio-and Soft Matter, Institute of Condensed Matter and Nanosciences, Université Catholique de Louvain, Croix du Sud 1, B-1348 Louvain-la-Neuve, Belgium*

M. Ahmadi

*Department of Polymer Engineering and Color Technology, Amirkabir University of Technology, Tehran, Iran and Bio-and Soft Matter, Institute of Condensed Matter and Nanosciences, Université Catholique de Louvain, Croix du Sud 1, B-1348 Louvain-la-Neuve, Belgium*

H. Goldansaz and E. van Ruymbeke<sup>a)</sup>

*Bio-and Soft Matter, Institute of Condensed Matter and Nanosciences, Université Catholique de Louvain, Croix du Sud 1, B-1348 Louvain-la-Neuve, Belgium*

(Received 22 June 2015; final revision received 12 January 2016; published 25 February 2016)

## Abstract

The linear viscoelastic properties of entangled hydrolysed poly(n-butyl acrylate) PnBA copolymers, with varying density of functional moieties, i.e., acrylic acid (AA) groups, have been investigated both experimentally and theoretically using small amplitude oscillatory shear and a modified version of the time marching algorithm (TMA). A second, low frequency, plateau, the level of which depends on temperature and AA groups content, is evident in the storage modulus of these copolymers. It indicates that terminal flow, i.e., chain motion at large length scales, is highly suppressed within the experimental timescale. This slow relaxation process is attributed to long lifetime aggregates (sticky junctions) of AA groups. At intermediate frequencies, the dynamic moduli decay with a slope of 0.5 indicative of a Rouse-like relaxation process. This behavior is well captured by the model when constraint release Rouse motion of the strands that are trapped between successive AA junctions or/and trapped entanglements is considered. One new parameter,  $p_{st}$ , the probability of a monomer to act as a sticky junction, is introduced in the TMA to account for the influence of the functional AA groups on the chain dynamics. The validation of this simple model is then achieved by comparing experimental and predicted viscoelastic data. © 2016 The Society of Rheology. [<http://dx.doi.org/10.1122/1.4942231>]

## I. INTRODUCTION

Associating polymers consist of polymer chains that carry functional groups. These functional groups are capable of forming transient interactions (noncovalent, temporal bonds), which provide a convenient control of the physical properties of this class of polymeric systems. For example, depending on the temperature or/and the concentration of functional groups, the rheological behavior of associative polymers ranges from rubberlike to liquidlike [1–3]. The origin of the temporal bonds varies: Among others, hydrogen bonding [4,5], ionic aggregation [6,7], and metal-ligand interactions [8] can all be considered as transient associations.

The large length scale (global) motion of an ordinary, nonassociating polymer chain is controlled by entanglements, the topological constraints experienced by a given chain due to the presence of the surrounding matrix chains. Typically, these constraints are modeled as a mean field tube to which a given (probe) chain is confined [9,10]. To escape

its entanglement constraints, a linear chain diffuses back and forth (reptates) along the axis of the confining tube (also known as the primitive path). In the terminal regime, which reflects the global motion of the chains, this relaxation process gives rise to a power law dependence of two and one for  $G'$  and  $G''$ , the storage and loss modulus, respectively, unless the system is characterized by substantial polydispersity. On the other hand, branched molecules such as star polymer chains relax their conformation via contour length fluctuations (CLFs) or arm retraction, the thermally activated fluctuations of the free ends of the primitive path [9,10]. (Note that early CLF also occur in linear chains until reptational modes eventually become the dominant relaxation process.)

Apart from the two aforementioned tube escape mechanisms, i.e., reptation and CLF, another process, namely, constraint release (CR), continually contributes to the orientation renewal of the polymer chains in the melt [10]. CR represents the loss of entanglements on a probe chain due to motion of the surrounding matrix chains. In tube models, it is often modeled by the dynamic tube dilution concept [11], according to which the relaxed part of the polymer acts as a solvent, and the effective tube diameter is growing as  $a \propto a_0 \Phi^{-\alpha/2}$  with  $\Phi$  being the “effective entanglement

<sup>a)</sup>Author to whom correspondence should be addressed; electronic mail: [evelyne.vanruymbeke@uclouvain.be](mailto:evelyne.vanruymbeke@uclouvain.be)

concentration” and  $\alpha$  being the so-called dilation exponent. Although there is some ambiguity on whether CR affects the global relaxation of monodisperse linear chains [12–14], it is well established that CR events significantly influence the chain dynamics in (i) binary blends of long and short linear chains [15] as well as (ii) in melts of monodisperse polymer stars [16]. With respect to system (i) above, due to the reptation (disentanglement/entanglement) process of the short chains, portions of the long chains located between two long-long entanglements make use of the extra freedom, undertake local hops, and eventually renew their conformation locally, at the rhythm of the entanglement/disentanglement of the short chains. This relaxation process approximately resembles the relaxation of a Rouse chain, and for this reason is often referred to as CR Rouse (CRR) process [15,17,18].

The above molecular view of orientation relaxation in polymer melts pays attention to the internal dynamics of the chains (entanglements and architecture). Of particular interest is how it changes when reversible (transient) bonds are present. The key quantity here is  $\tau_{ass}$ , the association lifetime (which depends on the strength of the reversible interaction): As shown by Lewis *et al.* [5], weak hydrogen-bonding associations like the ones formed between two acrylic acid (AA) groups have no marked influence on the viscoelastic properties since their association lifetime is fast compared to rheological chain relaxation. In contrast, strong interactions, encountered, for example, with ionic aggregates or with systems containing quadruple hydrogen bonds (UPy), strongly influence the chain dynamics above  $T_g$ , as the effective friction experienced by the polymer strands grows dramatically. This additional friction slows down the global relaxation of the chains and produces a wide spectrum of stress relaxation modes. For unentangled systems, these effects are typically captured by a modified Rouse model in which the friction is governed by the association lifetime [6,19]. A scaling theory of sticky reptation has been developed to model the dynamics of entangled associating polymers as well [1,20].

The aim of the present contribution is to investigate the combined effect of the dynamics of the associating groups (strength, position, and number) and the internal dynamics of the polymer chains (entanglements and architecture). A modified version of the time marching algorithm (TMA) is presented, and its predictions are compared against linear viscoelastic measurements on entangled hydrolysed poly(*n*-butyl acrylate) PnBA copolymers, with varying density of sticky groups. According to the adopted molecular picture, the AA sticky groups microphase separate from the PnBA matrix to form stable aggregates (sticky junctions) that play the role of transient junctions between different chains [21]. It must be noted that the lifetime of the aggregates is assumed to be drastically longer than the lifetime of a single hydrogen bond due to a single AA group. Thus global reorientation of chains that are attached to at least two aggregates is severely restricted. This molecular view is supported by the rheological data presented herein, *i.e.*, by the emergence of a second, low frequency plateau in  $G'$  (the level of this plateau depends on temperature and density of AA groups), and by dielectric measurements on the same samples [22].

We show that the modified TMA provides a reasonable fit to the rheological data, provided that CRR relaxation of the molecular strands between successive sticky junctions or/and trapped entanglements is incorporated in the model. This CRR equilibration is mediated by the unconstrained relaxation of the mobile components of the system, *i.e.*, by the normal relaxation (via reptation or/and CLF) of the polymer fractions that have at least one end not attached to sticky junctions. To determine the weight fractions and the molecular weight distributions (MWDs) of these mobile components, we follow a statistical approach that only introduces an extra parameter in the model, namely,  $p_{st}$ , the probability of a monomer to be attached to a sticky junction. The remainder of the article is structured as follows. Section II summarizes the experimental procedure while Sec. III presents the TMA for both ordinary and associating polymer melts (Subsections III A and III B, respectively). Section IV discusses thermorheological complexity and compares the model predictions with the experimental data. Conclusions are given in Sec. V.

## II. EXPERIMENTAL DETAILS

The materials studied in this work are the following: (i) A reference PnBA homopolymer with weight average molecular weight  $\bar{M}_w = 210$  kg/mol and measured polydispersity index (PDI) 1.3, (ii) a PnBA-PAA copolymer with 13% of AA active groups, and (iii) a PnBA-PAA copolymer with 38% of AA functional groups. The reported level of the AA groups was quantified by  $^1\text{H}$  NMR spectroscopy; however, it may be moderately overestimated owing to the complexity of the raw NMR data that made the peak assignment procedure nontrivial. According to the NMR measurements, the reference sample contains a small percent of functional groups evidenced as well by the extensional hardening behavior of this material [21]. Both copolymers were synthesized via hydrolysis of the reference PnBA homopolymer. Hence, all three samples have the same degree of polymerization  $N = 1641$ . Details of the synthesis are reported elsewhere [21,22]. Table I summarizes the molecular characteristics of the studied materials.

The glass transition temperature,  $T_g$ , of the samples was determined by differential scanning calorimetry measurements (DSC) [21]. It is influenced by the binary AA associations. As shown by Lewis *et al.* [5], the  $T_g$  of random PnBA-AA copolymers increases linearly with AA content; there, the AA groups form many binary associations that reduce segmental motion (by either decreasing the available free volume or increasing chain friction) near the glass transition

TABLE I. Molecular characteristics of the materials.

Sample	% of AA groups per chain	AA groups per chain	Entanglements per chain	$T_g$ (°C)	$N$
Reference PnBA	3	$\approx 49$	$\approx 12$	-51.0	1641
PnBA-AA13%	13	$\approx 207$	$\approx 12$	-49.5	1641
PnBA-AA38%	38	$\approx 615$	$\approx 12$	-47.0	1641

temperature. According to Table I, the Tg of our samples slightly rises with AA content, but clearly not in a linear fashion. A possible explanation for this disparity is the overestimation of the level of AA groups in our NMR analysis. Nevertheless, we believe that this discrepancy is due to microphase separation of the AA groups, as explained in detail below.

The distribution of AA groups at the hydrolysed samples is, most likely, blocky (short AA blocks along the PnBA backbone) rather than completely random. As shown by Nyrkova *et al.* [23], in such systems, the functional groups can microphase separate from the matrix forming distinct spherical nanodomains. (Here, PAA nanodomains are embedded in a PnBA matrix.) Dielectric measurements on the same samples also favor this scenario [22]; they reveal two glass transition temperatures, one corresponding to the PnBA matrix and a second one attributed to the PAA nanodomains. The phase separation scenario could also explain the nonlinear increase of the copolymers' Tg as a function of AA content. In DSC, both samples exhibit a single Tg implying that the volume fraction (and size) of the aggregates is relatively small as to produce a distinct signal, i.e., manifest an independent phase behavior. Compared to the system of Lewis *et al.*, at which many intermolecular binary associations occur, a milder increase in the samples' Tg is anticipated here since a high fraction of functional groups organizes in aggregates that constitute a rather small volume fraction of the system.

Another possibility is the formation of ionic clusters: In more detail, to remove potassium chloride (KCl) salt from the PnBA-AA systems, purified water has been used. Nevertheless, if the pH of the water is five or lower then carboxylate units are again formed. These units may form ion pairs with the cations that are present in the water. In turn, due to difference in polarity, the ion pairs phase separate from the polymer backbone to give ionic clusters (aggregates). Nevertheless, this possibility is rather unlikely since the samples showed very low metallic content under energy dispersive X-ray spectrometry (EDX) [21].

### III. MODELING

#### A. TMA for nonassociative polymers

The TMA is a tube based model that successfully predicts the linear viscoelasticity of ordinary, i.e., nonassociative, polymer melts [24–26]. It incorporates tube escape relaxation mechanisms, namely, reptation and CLF, as well as CR. In this model, the relaxation modulus,  $G(t)$ , reads

$$G(t) = G_N^0 F(t) + F_{LR} + F_{FR}, \quad (1a)$$

$$F(t) = \Psi(t)\Phi(t)^\alpha. \quad (1b)$$

In Eq. (1a),  $F_{LR}(t)$  and  $F_{FR}(t)$  denote, respectively, the contribution from the longitudinal and transverse Rouse modes [cf. Eqs. (8)]. The relaxation function,  $F(t)$ , accounts for both CR and tube escape: that is, in Eq. (1b),  $\Psi(t)$  is the fraction of polymeric material still unrelaxed by tube escape mechanisms after a waiting time  $t$ , while  $\Phi(t)$  is the contribution

coming from CR at the same timescale ( $1 - \Phi(t)$  corresponds to the material fraction that acts as a solvent at time  $t$ ). Following the dynamic dilution hypothesis [11], according to which the effect of CR events is modeled by considering that the unrelaxed polymer fraction relaxes in an effectively dilated tube,  $\Phi(t)$  is used to rescale  $M_e$ , the entanglement molecular weight (and in turn  $a$ , the tube diameter, and  $L_{eq}$ , the equilibrium length of the tube

$$M_e(t) = \frac{M_{e,0}}{\Phi(t)^\alpha}, \quad a(t) = \frac{a_0}{\Phi(t)^{\alpha/2}}, \quad L_{eq}(t) = L_{eq,0}\Phi(t)^{\alpha/2}, \quad (2)$$

with  $M_{e,0}$ ,  $a_0$ , and  $L_{eq,0}$  being the respective quantities in the absence of dynamic dilution (tube dilation). In the same equation,  $\alpha$  is the so-called tube dilation exponent that typically takes the values of 1 or 4/3; throughout this work it is fixed to 1. The method by which  $\Phi(t)$  is obtained in the TMA is as follows. At each time step, the unrelaxed material fraction,  $\Psi(t)$ , is first calculated [according to Eq. (4)]. Then,  $\Phi(t)$  is obtained by utilizing the following formula [24]:

$$\Phi(t) = \max \left[ \Psi(t), \Phi(t - \Delta t) \left( \frac{t - \Delta t}{t} \right)^{1/2\alpha} \right], \quad (3)$$

with  $\Phi(t = 0)$  being equal to unity. (In the above equation,  $\Delta t$  is the “simulation” time step.)

The unrelaxed material fraction is given by

$$\Psi(t) = \sum_{j=1}^m \nu_j \int_0^1 p_{rep}(x_i, t) p_{fluct}(x_i, t) dx_i, \quad (4)$$

where  $x_i$  is a normalized curvilinear variable that represents primitive path segments along a given arm  $j$ , and  $\nu_j$  is the volume fraction of each type of arm. (Note that linear chains are treated like star polymers with two arms.) In the same equation,  $p_{rep}(x_i, t)$  and  $p_{fluct}(x_i, t)$  denote the probabilities that the segment  $x_i$  survives by reptation and CLF, respectively; they are given by the following expressions:

$$p_{rep}(x_i, t) = \sum_{p \text{ odd}} \frac{4}{p\pi} \sin\left(\frac{p\pi x_i}{2}\right) \exp\left(\frac{-p^2 t}{\tau_d}\right), \quad (5a)$$

$$p_{fluct}(x_i, t) = \exp\left(\frac{-t}{\tau_{fluct}(x_i, t)}\right). \quad (5b)$$

Equation (5a) only refers to linear species. Here,  $\tau_d$  is the reptation time of the whole chain (a two arms star); it is given by  $\tau_d = \tau_{d,0}\Phi_{active}(t)^\alpha$  where  $\tau_{d,0}$  is the reptation time in the absence of tube dilation, and  $1 - \Phi_{active}(t)$  is the fraction of polymeric material acting as a solvent for the reptation process. (Throughout this work  $\Phi_{active}(t) = 1$ .) For arms of starlike chains, reptation is suppressed and thus  $p_{rep}(x_i, t)$  is practically unity. In this case, conformational relaxation of the primitive segments, by means of tube escape, solely occurs via CLFs. The CLF relaxation time of segment  $x_i$  at time  $t$ ,  $\tau_{fluct}(x_i, t)$ , is

$$\tau_{\text{fluct}}(x_i, t) = \begin{cases} \tau_{\text{early}}(x_i) & \text{for } x_i \leq x_{tr,j}, \\ \tau_{\text{early}}(x_{tr,j}) \exp\left(\frac{U(x_i, t) - U(x_{tr,j}, t)}{k_B T}\right) & \text{for } x_i > x_{tr,j}, \end{cases} \quad (6)$$

where  $\tau_{\text{early}}(y) = (9\pi^3/16)\tau_e Z_{a,j}^4 y^4$  is the explicit formula for the so-called early (shallow) CLF, with  $\tau_e$  and  $Z_{a,j}$  being the entanglement relaxation time of the polymer and the number of entanglements of arm  $j$ , respectively, in the absence of dynamic dilution (tube dilation). In Eq. (6),  $x_{tr,j}$  is the transition segment of arm  $j$ . It corresponds to the primitive segment at which the potential is of order of thermal energy, i.e.,  $U(x_{tr,j}) \approx k_B T$ , and it marks the transition from early to deep fluctuations. The potential energy is given by [26]

$$U(x, t) = 3k_B T Z_a \int_0^x \zeta \Phi(t(\zeta))^z d\zeta, \quad (7)$$

where  $\Phi(t(\zeta))$  is estimated according to Eq. (3). It corresponds to the unrelaxed polymer fraction at the timescale at which segment  $\zeta$  relaxes. Nevertheless, in this work dynamic dilution is modeled according to the original approach of McLeish [10], i.e., the unrelaxed fraction depends on time only implicitly (through the time dependence of  $\zeta$ ).

The explicit formulae for  $F_{LR}(t)$  and  $F_{FR}(t)$ , the Rouse relaxation functions in Eq. (1a), are [12]

$$F_{FR}(t, Z_{tot,j}) = \sum_j \frac{\rho R T}{M_{a,j}} \nu_j \left( \sum_{p=Z_{tot,j}}^{N_{a,j}} \exp\left(\frac{-2p^2 t}{\tau_{R_{a,j}}}\right) \right), \quad (8a)$$

$$F_{LR}(t, Z_{tot,j}) = \sum_j \frac{1}{5} \frac{\rho R T}{M_{a,j}} \nu_j \left( \sum_{p=1}^{Z_{tot,j}-1} \exp\left(\frac{-p^2 t}{\tau_{R_{a,j}}}\right) \right). \quad (8b)$$

In these equations, the quantities  $\rho$ ,  $R$ , and  $T$  are the polymer density, the gas constant, and the temperature, respectively;  $N_{a,j}$ ,  $M_{a,j}$ , and  $\tau_{R_{a,j}} (= \tau_0 N_{a,j}^2)$ , respectively, represent the degree of polymerization, the molecular weight, and the Rouse relaxation time of arm  $j$ . ( $\tau_0$  is the segmental relaxation time.)  $Z_{tot,j}$  is the total number of obstacles (constraints) acting on arm  $j$ ; for nonassociating chains  $Z_{tot,j} = Z_{a,j}$  since the only constraints are entanglements.

For monodisperse nonassociating chains, Eqs. (8) reduce to the expressions proposed by Likhtman and McLeish [12]. There, the contribution of the longitudinal modes to stress relaxation following a small shear deformation is analytically derived; the amplitude of the modulus of the longitudinal modes is five times smaller than the amplitude of the modulus of the transverse modes. The contribution of longitudinal modes was also addressed by Milner and McLeish in an earlier work [27], but via postulate rather than analytical calculation and so the prefactor for longitudinal modes was 1/3 instead of 1/5. Furthermore, Likhtman and McLeish argued that, for the transverse modes, a factor of 2 in the exponential exponent was missing in [27]. Note that longitudinal modes are not considered for the trapped strands (see Sec. III B 1 and Fig. 1 below). For this reason the lowest mode in Eq. (8b) is  $p = 1$ .

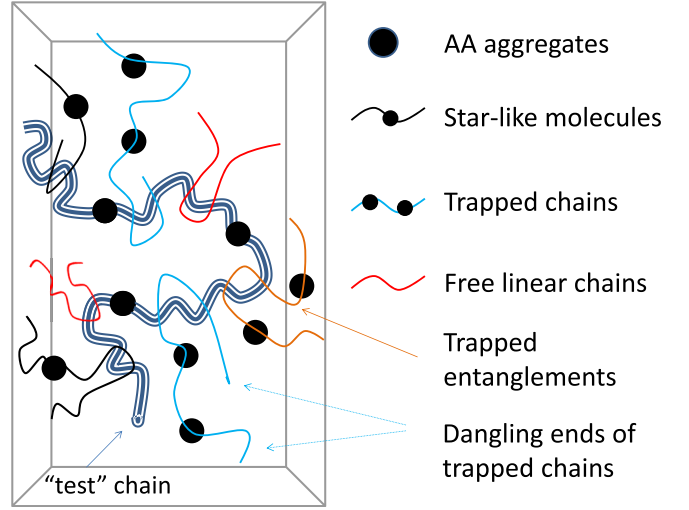


**FIG. 1.** Schematic illustration of the adopted physical picture. Aggregates (sticky junctions) of AA groups are shown as filled circles. A probe chain is shown. It is surrounded by free linear chains not attached to junctions, star-like chains that are only attached to one junction, and trapped chains that are connected to at least two junctions.

## B. Modeling the linear rheology of hydrolysed PnBA copolymers

In this section, the TMA model is modified in order to take into account the influence of the stickers along the chain. From the experimental data (cf. Figs. 5 and 8 below), several assumptions are made in order to build the model:

### 1. Assumptions

- The effect of single hydrogen bonding is neglected. In more detail, binary associations between different AA groups (AA dimers) are possible, however, their effect is ignored since their association lifetime is fast compared to rheological chain relaxation [5]. Apart from binary associations, other kinds of associated forms, such as linear oligomeric structures, are possible between AA groups [28]; these nonbinary associations are also disregarded in the model.
- The deviation of the rheological data from the typical slopes of one and two at low frequencies for  $G''$  and  $G'$ , respectively, as well as the low level of the second plateau for PnBA-AA38 (cf. Figs. 5, 7, and 8 below) imply that the chains contain a few transient bonds that have very long lifetime, i.e., a lifetime that is much longer than the average disentanglement time of the chain as well as the average lifetime of a hydrogen bond due to an AA dimer (binary associations). In our view, the mechanism which is responsible for the long lifetime bonds formation is the collective assembly (microphase separation) of the functional groups in distinct PAA nanodomains. Here, we assume that the lifetime of these nanodomains is infinite. As discussed in Sec. IV B, this hypothesis is not valid anymore at very high temperatures.
- As observed in the storage modulus, the level of the second plateau is rather low, which means that only a small fraction of chains is trapped into the transient network and is not able to relax. This is in agreement with the

observation that the plateau modulus of the hydrolysed samples does not show large increase, being mainly dependent on the entanglements, not on the stickers. We therefore assume that the samples contain few stickers compared to the number of entanglements per chain.

- The samples are considered monodisperse (see Sec. IV B).

With the aforementioned measurements in mind, we adopt the following physical picture, illustrated schematically in Fig. 1. The polymer fraction is divided into mobile and trapped components. In particular, we consider four different types of chains: (i) Free linear chains that are not attached to aggregates, but keep their extremities free to move, (ii) starlike chains that are attached to only one long lifetime sticker, (iii) trapped stands of chains that are connected to at least two aggregates, and (iv) dangling ends of the trapped chains. Free linear chains, starlike molecules, and dangling branches of the trapped chains constitute the mobile polymer fraction of the system as they are able to relax by tube escape mechanisms. In contrast, sections of trapped chains between two extreme sticky junctions are essentially immobile since renewal of their global configuration is restrained until dissociation of the long lifetime stickers. Hereafter, the volume fractions of chains (i)–(iv) above will be denoted as  $\nu_f$ ,  $\nu_s$ ,  $\nu_t$ , and  $\nu_d$ , respectively. They will be determined by a statistical approach, detailed in Sec. III B 3 below, from the value given to  $p_{st}$ , the probability to find a sticker along the chain. Figure 1 also illustrates a trapped entanglement; such entanglements will be considered as sticky junctions in the model since their lifetime will be of the same order as the lifetime of the sticky junctions.

## 2. Relaxation modulus

In order to determine the relaxation modulus, several relaxation steps can be pointed out through time. These steps are illustrated in Fig. 2. Specifically:

- (i) At early timescales Rouse motion occurs, which involves motion of subchains of increasing lengths. The signature of this motion at the dynamic moduli vs

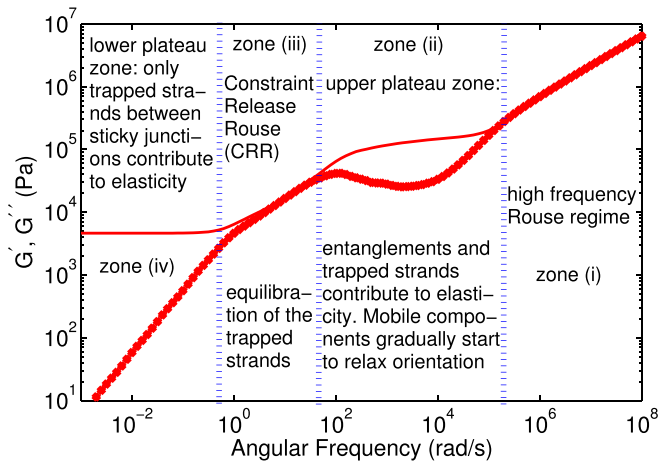


FIG. 2. A graphical illustration of the four relaxation regimes (zones) considered in the model. The different zones are discussed in the text. The solid curve corresponds to  $G'$  while the dotted one to  $G''$ .

frequency plot is the downward-sloping line with a slope of  $-1/2$  on a log-log scale at high frequencies. The transition to the upper (first) plateau zone marks the saturation of the Rouse modes, and the tube picture starts to be relevant; in other words, the length of the subchains reaches the average spacing between two entanglements or long lifetime stickers. At these short times, the relaxation modulus is therefore well described as

$$G(t) = G_{N,total}^0 + G_R(t), \quad (9)$$

where the plateau modulus,  $G_{N,total}^0$ , describes the high frequency part of zone (ii), and it is determined by accounting for both entanglements and sticky junctions [20]. Thus,

$$\begin{aligned} G_{N,total}^0 &= \frac{4}{5} \frac{\rho RT}{M_{e,total}} = \frac{4}{5} \frac{\rho RT}{M} Z_{tot} \\ &= \frac{4}{5} \frac{\rho RT}{M} \left( \frac{M}{M_{e,ent}} + \frac{M}{M_{e,XX}} \right), \end{aligned} \quad (10a)$$

$$M_{e,total}^{-1} = M_{e,ent}^{-1} + M_{e,XX}^{-1}, \quad (10b)$$

where  $M$  represents the molecular weight of the chain and  $Z_{tot}$  is the total number of obstacles (ordinary and frozen entanglements, and sticky junctions) acting on the whole chain. The quantity  $M_{e,XX}$  represents the molecular weight between sticky junctions [see also Sec. III B 3 and Eq. (19) below].  $M_{e,total}$  denotes the average molecular weight between two adjacent constraints of any kind, i.e., entanglements, sticky junctions, and trapped entanglements (see Figs. 1 and 3).  $M_{e,ent}$  is the entanglement molecular weight, given by

$$G_{N,ent}^0 = \frac{4}{5} \frac{\rho RT}{M_{e,ent}}. \quad (11)$$

The function  $G_R(t)$  in Eq. (9) is the contribution from the Rouse modes. In particular,

$$G_R(t) = F_{FR} + F_{LR}, \quad (12)$$

with  $F_{FR}$  and  $F_{LR}$  being given in Eqs. (8).

- (ii) Then, as a second relaxation step, the dangling branches of the trapped chains as well as the starlike chains will renew orientation by CLF. Moreover, the free linear chains will relax by reptation and CLF. During this relaxation step, the relaxation modulus can therefore be described as

$$G(t) = G_{N,total}^0 [\nu_m \Psi_m(t) (\nu_m \Psi_m(t) + \nu_t)^\alpha + \nu_t \Psi_t], \quad (13)$$

where  $\alpha$  is the dilation exponent, and  $\nu_m$  is the volume fraction of the mobile components: that is, free linear chains, starlike chains, and dangling ends of trapped chains. (Hence,  $\nu_m = 1 - \nu_t = \nu_f + \nu_s + \nu_d$ .) At this time scale,  $\Psi_t$ , the tube survival probability of the trapped polymer fraction is always equal to unity

since tube escape mechanisms, i.e., either reptation or CLF, are quenched in the trapped strands.  $\Psi_m$  is the overall tube survival probability of the mobile polymer fraction. It is given in Eq. (4). We note however

that, in this case, Eq. (4) must be divided by  $v_m$  to ensure that the values of  $\Psi_m$  lie between zero and unity. In calculating  $\Psi_m$ , we use the following expression in Eq. (7) [29,30]:

$$\Phi(\xi) = \begin{cases} \nu_t + \nu_f(1 - \xi) + \nu_s \left( 1 - \sqrt{\frac{\overline{M}_{w,f}}{2\overline{M}_{w,s}} \xi} \right) + \nu_d \left( 1 - \sqrt{\frac{\overline{M}_{w,f}}{2\overline{M}_{w,d}} \xi} \right) & \text{linear,} \\ \nu_t + \nu_f \min \left[ \left( 1 - \sqrt{\frac{\overline{M}_{w,s}}{2\overline{M}_{w,f}} \xi} \right), \exp\left(-\frac{t}{\tau_d}\right) \right] + \nu_s(1 - \xi) & \\ + \nu_d \left( 1 - \sqrt{\frac{\overline{M}_{w,s}}{2\overline{M}_{w,d}} \xi} \right) & \text{stars,} \\ \nu_t + \nu_f \min \left[ \left( 1 - \sqrt{\frac{\overline{M}_{w,d}}{2\overline{M}_{w,f}} \xi} \right), \exp\left(-\frac{t}{\tau_d}\right) \right] + \nu_s \left( 1 - \sqrt{\frac{\overline{M}_{w,d}}{2\overline{M}_{w,s}} \xi} \right) & \\ + \nu_d(1 - \xi) & \text{dangling.} \end{cases} \quad (14)$$

Furthermore, while equation Eq. (13) takes into account the Dynamic Dilution effect of the mobile polymer fraction, it is assumed that at this time scale the trapped strands do not have the required time to explore their dilated tube (which represents the third step of relaxation), i.e.,  $\Psi_t = 1$ . Indeed, with such a system, the sticky junctions suppress the possible monomeric tension equilibration along the chain [31], which allows the chain to move through the remaining entanglements. As a consequence, the trapped portions can only relax by laterally exploring the dilated tube. This equilibration can only occur by a CRR motion [31] at the rhythm of the blinking of the entanglements of the mobile polymer fraction. As described in (iii) below we assume that the time regime for CRR motion will take place after the relaxation of the mobile fractions. Hence, at time scales corresponding to zone (ii), we will ignore the CRR relaxation of the trapped strands; in the model, this process only occurs in zone (iii).

- (iii) Once the mobile components have relaxed, i.e., when all the entanglements of the mobile sections are relaxed, the CRR process becomes active. Trapped strands between successive sticky junctions partially renew configuration through local CRR events. (That is, the segments of the trapped strands will undertake Rouse-like hops.) These events occur at the rate at which chain ends of the mobile fractions pass through the trapped chain portions, i.e., at a rhythm determined by the rate at which entanglements between the trapped strands and the surrounding mobile material disappear/reappear. They provide extra freedom

to the trapped strands, which can now explore the surrounding space on a larger length scale than the one corresponding to the original tube diameter (that is, the tube defined by all entanglements between a given trapped chain and the mobile matrix chains). Notice that the different renewal rates of the mobile fractions naturally give rise to a continuous spectrum of hopping rates. The TMA could in principle be adjusted to allow the CRR process to occur simultaneously with the relaxation of the mobile components. Nevertheless, such a calculation, i.e., the incorporation of a continuous spectrum of hopping rates, is beyond the scope of this work; for the sake of simplicity, a single average rate will be used in this simple model [see Eq. (22)].

The explicit expression for describing the CRR mechanisms is as follows:

$$G_{CR,R}(t) = G_{N,trapped}^0 \sum_{p=1}^{N_{ent}} \exp\left(\frac{-2p^2 t}{\tau_{CR,R}}\right), \quad (15)$$

where  $G_{N,trapped}^0$  is the second plateau modulus that follows the CRR process; it corresponds to  $M_{e,trapped}(=M_{e,total}/\nu_t^\alpha)$ , and its value is defined as

$$G_{N,trapped}^0 = \frac{4}{5} \frac{\rho RT}{M_{e,trapped}} \nu_t = \frac{4}{5} \frac{\rho RT}{M_{e,total}} \nu_t^{\alpha+1} = G_{N,total}^0 \nu_t^{\alpha+1}. \quad (16)$$

The timescale  $\tau_{CR,R}$  is the CRR equilibration time. It is given by  $\tau_{CR,R} = \tau_{obs} N_{ent}^2$  with  $N_{ent}(=v_t^{-\alpha} - 1)$  being the average number of entanglement segments per subchains confined between two sticky junctions or/and trapped entanglements. Here,  $\tau_{obs}$  is the average relaxation time of the mobile

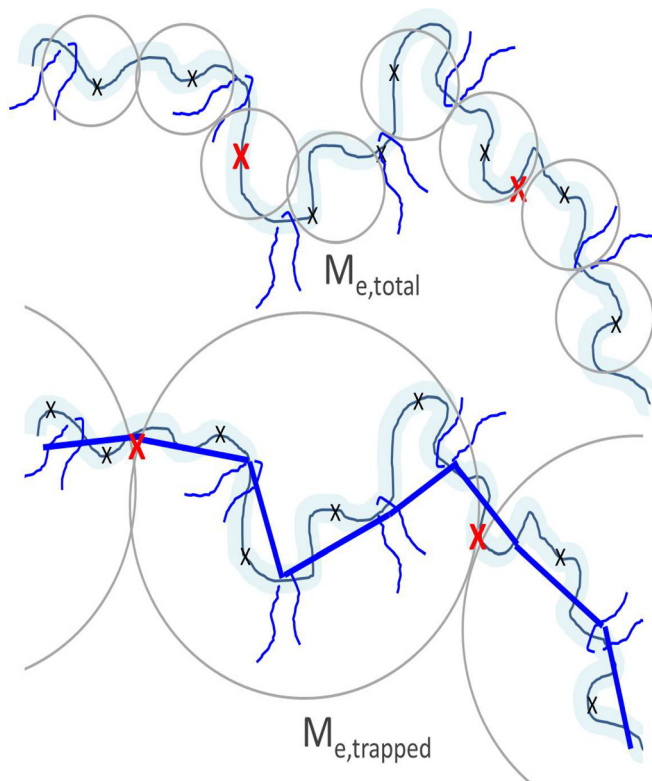


**FIG. 3.** Cartoon of the relaxation mechanisms of a probe chain (thick line). Large crosses indicate sticky junctions or/and trapped entanglements while small crosses represent AA groups that are not attached to the junctions. Upper: At early timescales, the mobile components (thin lines) are still entangled with the probe chain. The “relaxation blob” is defined by both sticky junctions and entanglements. Relaxation occurs via pure Rouse motion only. Bottom: At later times, the mobile components act as solvent, i.e., they renew their configuration much faster than the probe so that the relaxation blob is only defined by the large crosses. Chain portions of the probe between adjacent sticky junctions or/and trapped entanglements can relax orientation via CRR equilibration. The average molecular weight of these strands is  $M_{e,trapped}$ .

polymer fractions (thus,  $\tau_{obs}^{-1}$  is the average rate of the local CRR hops). It is determined by averaging the terminal relaxation time of the mobile components [Eq. (22)].

Another source of stress relaxation in associating solutions or melts where aggregates of functional groups are formed is the so-called hopping or partner exchange process [1,32,33]. In this process, the functional groups hop randomly between aggregates. Here, each hop allows stress relaxation in the portion of chain bearing the functional group, in a similar fashion to stress relaxation via CRR. Therefore, one would expect a competition between these two mechanisms. We argue that CRR dominates over the hopping mechanism in entangled systems at which: (i) A substantial fraction of the polymeric material is mobile and, in turn, the average number of aggregates per chain is small, and (ii) the lifetime of these aggregates is much longer compared to rheological chain relaxation. Our reasoning is as follows: Compared to systems with many aggregates, a given trapped stand, in our case, is on average longer and, moreover, it is surrounded by more mobile polymer fraction therefore its local relaxation is controlled by the disentanglement/entanglement blinking rather by the partner exchange process. The latter process should dominate over CRR when

there are aggregates per chain and the fraction of mobile components is low.

- (iv) The terminal relaxation of the trapped chains is delayed until dissociation of the sticky junctions takes place. As mentioned earlier in most cases it is outside the experimental window, so we simply consider this terminal relaxation time as infinite. Nevertheless, the beginning of this regime can be observed with specific samples at high temperatures. In such a case, we simply consider a Maxwell behavior

$$X(t) = \exp\left(\frac{-t}{\tau_{ass}}\right), \quad (17)$$

with  $\tau_{ass}$  being the association time of the long lifetime stickers.

Summarizing the above four regimes the final expression for the relaxation modulus,  $G(t)$ , reads

$$G(t) = G_R(t) + G_{N,total}^0 [\nu_m \Psi_m(t) (\nu_m \Psi_m(t) + \nu_t)^\alpha] + G_{CRR}(t) + G_{N,trapped}^0 X(t), \quad (18)$$

where  $G_R(t)$ ,  $G_{CRR}(t)$ , and  $X(t)$  are given in Eqs. (12), (15), and (17), respectively, while parameters  $G_{N,total}^0$ ,  $G_{N,trapped}^0$ ,  $M_{e,total}$ ,  $M_{e,XX}$ ,  $M_{e,trapped}$ ,  $\nu_f$ ,  $\nu_s$ ,  $\nu_d$ ,  $\nu_t$ , and  $\tau_{obs}$  are all determined from,  $p_{st}$ , the only fit parameter (see Sec. III B 3) as well as the normal parameters of the reference PnBA chain. Equation (18) does not double count modes; beyond the high frequency Rouse regime and prior to any molecular relaxation of the mobile material, it reduces to  $G_{N,total}^0$  as it should.

### 3. Statistical position of the long lifetime stickers along the chain

To use the model developed in Subsection III B 2, several quantities still need to be determined. This is achieved with the help of only one additional fit parameter, namely,  $p_{st}$ , the probability that a monomer behaves like a sticky junction. Specifically, using  $p_{st}$ , and the statistical approach explained below, we have determined (i) the proportion of mobile and trapped components, i.e., the volume fractions  $\nu_f$ ,  $\nu_s$ ,  $\nu_d$ , and  $\nu_t$ , (ii) the average molecular weight between successive sticky junctions,  $M_{e,XX}$ , (iii) the average molecular weight between sticky junctions or/and trapped entanglements,  $M_{e,trapped} (= M_{e,total} / \nu_t^\alpha)$ , (iv) the average molecular weight (length) of the mobile and nonmobile components as well as their MWDs, and (v) the average relaxation time of the mobile components,  $\tau_{obs}$ .

In more detail, chains are considered monodisperse, and each of them contains 1641 monomers, corresponding to the average molecular weight of the reference PnBA sample. All monomers along the chain are then examined in order to determine in a statistical way whether they behave as a sticky point or not: that is, a random number in the range [0,1] is compared to  $p_{st}$ , and if its value is lower than  $p_{st}$  the monomer is considered to act as a sticky junction (long lifetime sticker). Then the polymeric material is classified into four categories: (1) Free, linear chains, (2) starlike

chains (i.e., containing only one sticker), (3) trapped strands (i.e., molecular segments which are trapped between the two extreme aggregates of chains containing at least two aggregates), and (4) dangling branches attached to the trapped strands (see Fig. 1). By summing up the number of monomers in each of these categories, we readily determine their relative weight/volume proportions, i.e., we obtain the volume fractions  $\nu_f$ ,  $\nu_s$ ,  $\nu_d$ , and  $\nu_t$ . Figure 4(a) shows, for various values of  $p_{st}$ , the chains distribution as a function of the number of sticky junctions. Three different values of  $p_{st}$  are shown;  $p_{st} = 1/100$  (diamonds),  $p_{st} = 1/500$  (circles), and  $p_{st} = 1/1500$  (squares). As it is readily seen from this plot, decreases in the value of  $p_{st}$  lead to narrower distributions, and chains with fewer sticky junctions are obtained; for  $p_{st} = 1/1500$ , for example, the most probable structures are free linear chains and molecules containing only one sticker (starlike).

$M_{e,XX}$ , the average molar mass of a segment between two long lifetime stickers, is determined from the statistical approach: Here, chains are not classified according to the number of sticky points they contain, but they are considered as an infinite linear chain; for this infinite chain, the average molecular weight of all branches between stickers is estimated, and this value is used for  $M_{e,XX}$ . The estimated value is in accordance with the Flory result

$$M_{e,XX} = M_0 \frac{(2 - p_{st})}{p_{st}}, \quad (19)$$

where  $M_0$  is the monomeric molar mass. (Throughout this paper, we have used  $M_0 = 128\text{g/mol}$ , the molar mass of the unfunctionalized monomers.)

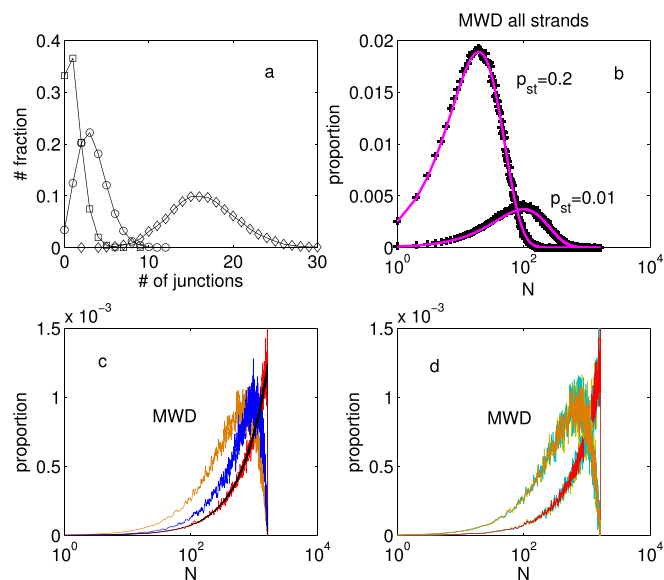


**FIG. 4.** Panel (a): Volume fractions of chains vs the number of sticky junctions per chain for three different values of  $p_{st}$ ; in particular,  $p_{st} = 1/100$  (diamonds),  $p_{st} = 1/500$  (circles), and  $p_{st} = 1/1500$  (squares). Panel (b): The obtained MWD for all possible strands (symbols). The lines show the anticipated Flory MWD. Panel (c): For  $p_{st} = 1/1500$ , the MWD of the starlike chains (right), of the dangling arms (left), and of the trapped strands (middle). Panel (d): The MWD of the stars and of the dangling arms, as in panel (c), as well as the MWD of their left and right strands separately.

The average molecular weights (molar masses) of components (1)–(4) above as well as their MWDs have been evaluated as follows. For each category, we obtain  $n_N$ , the number fraction of strands containing  $N$  monomers, and  $w_N$ , the corresponding weight fraction, by utilizing the following equations:

$$n_N = \frac{\Omega_N}{\sum_{N=1}^{\infty} \Omega_N}, \quad \text{and} \quad w_N = \frac{n_N N}{\sum_{N=1}^{\infty} n_N N}, \quad (20)$$

where  $\Omega_N$  denotes the number of strands with degree of polymerization  $N$ . [In practice, the sum in Eq. (20) extends from  $N = 1$  to  $N = 1641$ .] Knowing  $n_N$  and  $w_N$ , it is straightforward to obtain the MWDs of the different strands as well as the MWD of all strands between sticky junctions in the system.

As an example, in Fig. 4(b) we present (symbols) the obtained MWD of all possible strands for two different values of  $p_{st}$ , i.e.,  $p_{st} = 0.2$  and  $p_{st} = 0.01$ . When  $p_{st} = 0.2$ , the probability of a monomer acting as a sticky junction is higher therefore the system contains shorter branches compared to the case at which  $p_{st} = 0.01$ . In both cases, due to the large values of  $p_{st}$ , the system consists of trapped chains mainly, and the MWD follows the Flory distribution, i.e., the weight fractions obey the following expression:  $w_F(N) = N(1 - p_{st})^{N-1}(p_{st})^2$ . However, with decreasing  $p_{st}$ , free and starlike chains outnumber the trapped ones and the MWD is no longer Flory, the chain length being monodisperse.

In Fig. 4(c), we present the MWD of the starlike chains (right), of the dangling arms (left), and of the trapped strands (middle) for  $p_{st} = 1/1500$ . The horizontal axis corresponds to number of segments. (Since the free linear chains are considered monodisperse their MWD is not shown.) In the same panel, the thin line shows the MWD of the starlike chains when a different statistical approach is considered (that is, we randomly decide which of the 1641 monomers behaves as a sticky junction and then we calculate the MWD of the arms considering three million starlike chains). In Fig. 4(d), we also present the obtained MWDs when the “left” and “right” arms of the starlike chains are considered separately (also for the left and right dangling ends of the trapped chains). It is evident that for both cases the two end strands have similar MWD as it should be. Note that none of the MWDs presented in Figs. 4(c) and 4(d) is Flory because the value of  $p_{st}$  is low and the backbones are monodisperse. Hence, the vast majority of polymeric material comprises free and starlike arms which have a PDI of unity and 1.3, respectively. Sawtooth oscillations in the curves of Figs. 4(c) and 4(d) are due to the number of chains considered in the statistical approach. All calculations in this paper have been performed using 80 thousand chains; at the expense of computational time, smoother curves for the MWDs can be obtained considering more chains, however, the values of  $\bar{M}_w$  and polydispersity reported in Tables II and III do not change. The volume fractions of the mobile and trapped components slightly change, without a noticeable effect on the rheological response nevertheless.

**TABLE II.** Parameterization for the PnBA-AA13 copolymer.

Type of chain	Input	$p_{st} = 1/2900$	$p_{st} = 1/3100$	$p_{st} = 1/3400$	$p_{st} = 1/3600$	$p_{st} = 1/4000$	$p_{st} = 1/4300$
(1) Free linear	$\nu_f$	0.57	0.59	0.61	0.63	0.66	0.68
	$\bar{M}_w$ (kg/mol)	210	210	210	210	210	210
	PDI	1	1	1	1	1	1
(2) Starlike	$\nu_s$	0.32	0.31	0.30	0.29	0.28	0.27
	$\bar{M}_w$ (kg/mol)	140	140	140	140	140	140
	PDI	1.3	1.3	1.3	1.3	1.3	1.3
(3) Trapped	$\nu_t$	0.04	0.04	0.03	0.03	0.02	0.02
	$\bar{M}_w$ (kg/mol)	110	110	110	110	109	109
	PDI	1.5	1.5	1.5	1.5	1.5	1.5
(4) Dangling ends	$\nu_d$	0.07	0.06	0.06	0.05	0.04	0.03
	$\bar{M}_w$ (kg/mol)	102	102	102	102	103	103
	PDI	1.5	1.5	1.5	1.5	1.5	1.5
	$M_{e,trapped}$ (kg/mol)	430	466	566	630	780	852
	$\tau_{obs}$ [Eq. (22)]	0.67s	0.66s	0.65s	0.64s	0.62s	0.61s

The number and weight average molar mass of each component,  $\bar{M}_N$  and  $\bar{M}_w$ , respectively, are calculated through the following expressions:

$$\bar{M}_N = \sum_{N=1}^{\infty} n_N M_N, \quad \text{and} \quad \bar{M}_w = \sum_{N=1}^{\infty} w_N M_N, \quad (21)$$

with  $M_N (= M_0 N)$  being the molar mass of a chain with  $N$  monomers, and  $M_0$  being the monomeric molar mass. Tables II and III present the obtained  $\bar{M}_w$  for all chain types and specific values of  $p_{st}$ , which have been determined by best fitting procedure in comparison to experimental data of the hydrolyzed copolymers (cf. Sec. IV B, Figs. 7 and 8). In the same tables, volume fractions and PDIs are also shown. In contrast to volume fractions, PDI and average molecular weights are rather insensitive to variations of  $p_{st}$ , for the range of values used here. Note that, for the PnBA-AA38 case, the trapped volume fractions constitutes of chains containing two, three, and four sticky junctions; here,  $\bar{M}_w$  of the trapped strands corresponds to the average molecular weight between the two extreme sticky junctions. For the PnBA-AA13 copolymer, the trapped volume fraction consists of chains containing two aggregates only.

The obtained volume fractions and molecular weights are then used for the estimation of  $\tau_{obs}$ , the average relaxation time of the mobile fractions; more specific  $\tau_{obs}$  is calculated according to

$$\tau_{obs} = \nu_f \tau_{df} + \nu_s \tau_{fluct,s} + \nu_d \tau_{fluct,d}, \quad (22)$$

where  $\tau_{df}$  is the reptation time of the free, linear chains. In the same equation,  $\tau_{fluct,s}$  is the average time taken for complete relaxation via CLF of the arms of the starlike chains, i.e., the time taken for an arm tip to reach the sticky junction, while  $\tau_{fluct,d}$  is the average relaxation time for the dangling arms of the trapped chains. It must be noted that in reality there is a distribution of times associated with the relaxation of the mobile polymer fraction, which is not taken into account in the present model.

At this point, applying the proposed model [Eq. (18)] to the two hydrolyzed copolymers only requires the values of the three typical parameters of the original TMA for the reference sample, i.e.,  $M_{e,ent}$ ,  $G_{N,ent}^0$ , and  $\tau_e$ . These parameters are defined in Sec. IV B. Before doing this, however, we discuss the thermo-rheological behavior of all three samples.

**TABLE III.** Parameterization for the PnBA-AA38 copolymer.

Type of chain	Input	$p_{st} = 1/1400$	$p_{st} = 1/1450$	$p_{st} = 1/1500$	$p_{st} = 1/1600$	$p_{st} = 1/1700$	$p_{st} = 1/2000$
(1) Free linear	$\nu_f$	0.31	0.32	0.34	0.36	0.38	0.44
	$\bar{M}_w$ (kg/mol)	210	210	210	210	210	210
	PDI	1	1	1	1	1	1
(2) Starlike	$\nu_s$	0.36	0.36	0.36	0.37	0.37	0.36
	$\bar{M}_w$ (kg/mol)	140	140	140	140	140	140
	PDI	1.3	1.3	1.3	1.3	1.3	1.3
(3) Trapped	$\nu_t$	0.13	0.13	0.12	0.11	0.10	0.08
	$\bar{M}_w$ (kg/mol)	117	117	115	116	115	113
	PDI	1.4	1.4	1.4	1.4	1.4	1.4
(4) Dangling ends	$\nu_d$	0.20	0.19	0.18	0.16	0.15	0.12
	$\bar{M}_w$ (kg/mol)	99	98	99	99	99	101
	PDI	1.6	1.6	1.6	1.6	1.6	1.5
	$M_{e,trapped}$ (kg/mol)	126	132	143	156	172	228
	$\tau_{obs}$ [Eq. (22)]	0.81s	0.81s	0.81s	0.8s	0.76s	0.75s

## IV. RESULTS AND DISCUSSION

### A. Master curves and thermo-rheological complexity

The master curves of the reference sample and the PnBA-AA13 copolymer are shown in Fig. 5(b). They are obtained using the horizontal shift factors,  $a_T$ , presented in Fig. 5(a). These shift factors clearly exhibit a Williams-Landel-Ferry (WLF) behavior (black line), i.e., they obey the equation  $\log a_T = -C_1(T - T_0)/(C_2 + T - T_0)$  where  $C_1 = 5.244$ ,  $C_2 = 159.14$ , and  $T_0 = 45^\circ\text{C}$  (the so-called reference temperature). Both master curves superimpose very well at high frequencies, displaying the same Rouse dynamics at this reference temperature. (Close to the glass transition temperature the Rouse dynamics can be affected as binary AA associations are active [22].) From this, we conclude that the sticky groups along sample PnBA-AA13 do not strongly affect the local dynamics of the chains. Furthermore, we observe that both curves show the same level of plateau modulus: Apparently, the proportion of sticky junctions in sample PnBA-AA13 is too low to significantly affect the upper plateau modulus and, moreover, give rise to a clear second plateau at lower frequencies. However, the sticky junctions seem to slow down the terminal relaxation of the material, with an influence which depends on temperature, producing large thermo-rheological complexity (TRC) at low frequencies. On the other hand, although the reference sample contains a small percentage (3%) of functional AA groups, it clearly exhibits a simple thermo-rheological behavior over the whole frequency range.

Building a master-curve for the PnBA-AA38 copolymer is more delicate since this sample manifests TRC also at intermediate frequencies. In order to follow a consistent approach, the data of the PnBA-AA38 sample have been shifted according to the shift factors of the reference and PnBA-AA13 samples. Furthermore, all the curves have been

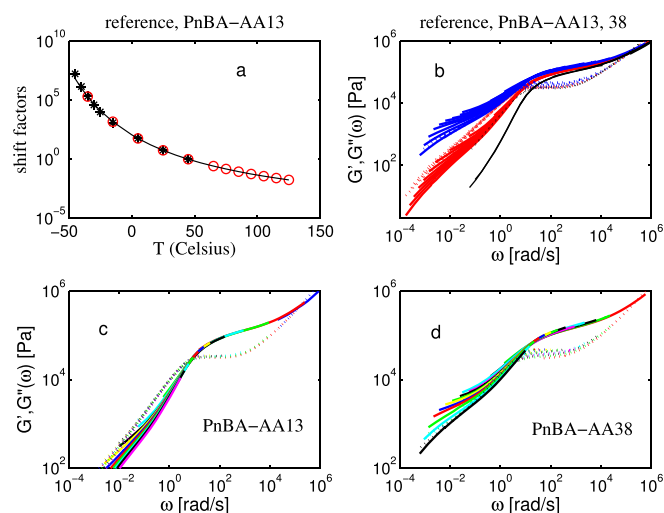


**FIG. 5.** Panel (a): Asterisks and open circles are the horizontal shift factors for the reference and PnBA-AA13 copolymer, respectively. The line corresponds to the WLF equation. Panel (b): The master curves of the reference (right), PnBA-AA13 (middle), and PnBA-AA38 (left) samples at a reference temperature of  $45^\circ\text{C}$ . Panels c and d: For better illustration, the master curves of PnBA-AA13 and PnBA-AA38 are shown separately.

horizontally shifted to larger frequencies by a constant factor, in order to ensure that the high frequency cross-over superimpose with the respective cross-over of the other samples. (That is, the WLF shift factors determined from the reference and the PnBA-AA13 copolymer are all multiplied by a factor 2.5) This shift is, most likely, due to the different glass transition temperature of this sample (see Table I). The corresponding master curve is presented in the upper, right panel of Fig. 5 with blue lines. It shows TRC at both intermediate and high frequencies. For better illustration, the master curves of the PnBA-AA13 and PnBA-AA38 copolymers are separately shown at the bottom panels of Fig. 5. It should be stressed that all master curves presented in Fig. 5 are build without applying a vertical shift.

TRC implies a failure of the time-temperature superposition (tTS) principle. Such a failure is often observed in associating polymers [2,34]. The physical origin of this failure is attributed to the different temperature dependence of the chain relaxation time (which follows the temperature dependence of  $\tau_e$ ) and the association lifetime,  $\tau_{ass}$ , and consequently the average number of associated stickers. That is, the motions of the chains are dictated by two different processes: (i) Dynamics of stickers and (ii) reorientation of the entanglement segments (disentanglement), which have different temperature dependence.

Both copolymers exhibit TRC at low frequencies. This is because the terminal flow is affected by the long lifetime stickers; here, the dynamics are determined by both disentanglement and the dynamics and number of the long lifetime stickers. With respect to intermediate frequencies, PnBA-AA38 manifests TRC. This behavior may be due to the rapid association/dissociation process of binary AA associations, which is neglected here but it is considered in an accompanying work [35], or due to a distribution of lifetimes of the sticky junctions. On the other hand, PnBA-AA13 is thermo-rheologically simple at these frequencies. This behavior is attributed to the much lower content of stickers compared to PnBA-AA38: With fewer stickers the distribution of lifetimes of the sticky junctions is expected to narrow; also, less binary associations are anticipated in PnBA-AA13 than in PnBA-AA38.

### B. Comparison with experiments

The plateau modulus of the reference sample has been determined by best fitting procedure using the ordinary TMA approach [Eq. (1a)] leading to  $G_{N,ent}^0 = 160$  kPa. This value corresponds to an entanglement molecular weight of 17.5 kg/mol since  $G_{N,ent}^0$  and  $M_{e,ent}$  are related through Eq. (11). Both values seem reasonable compared to literature values [36]. The last material parameter,  $\tau_e$ , has been fixed to  $7.5 \times 10^{-5}$  at  $45^\circ\text{C}$  based on the inverse of the high frequency cross-over between  $G'$  and  $G''$ . The corresponding theoretical curves (lines) are compared against the master curve of the reference sample (symbols) in Fig. 6. Here, the solid and dotted lines refer to polydispersity of 1 and 1.3, respectively. It is obvious that, in the terminal regime, a PDI of 1.3 leads to a better agreement between the predicted and experimental

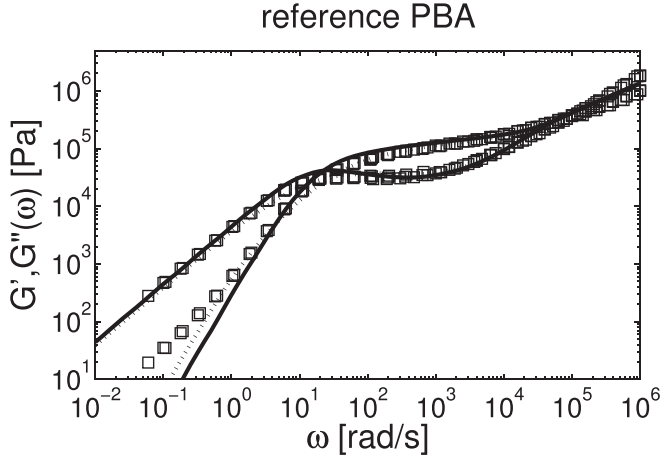


**FIG. 6.** Symbols represent the experimental loss and storage moduli of the reference sample while lines correspond to theoretical predictions for  $PDI = 1$  (solid) and  $PDI = 1.3$  (dotted).

curves. Nevertheless, the agreement found by considering the sample as monodisperse stays acceptable. For this reason, and to keep the modified TMA model as simple as possible, the PnBA-AA copolymers are considered monodisperse.

The discussion now turns to the hydrolyzed PnBA-AA samples. Figures 7 and 8 compare the modified TMA approach [Eq. (18)] and the experimental data of PnBA-AA13 and PnBA-AA38, respectively. Apart for the very low temperatures ( $-35^\circ\text{C} < T < -5^\circ\text{C}$ ), each temperature is examined separately as tTS fails for these materials. For each temperature we determine the best fit value of  $p_{st}$ , the only fit parameter. These values are shown in Fig. 9 as a function of temperature for both copolymers. From this figure, one readily observes that  $p_{st}$  decreases with increasing temperature, as expected. The values of  $p_{st}$  appear to follow a single exponential decay:  $y = y_0 + A \exp(-T/B)$ , where  $y_0 = 4.1 \times 10^{-4}$  ( $7.3 \times 10^{-4}$ ),  $A = -7.6 \times 10^{-5}$  ( $-2.5 \times 10^{-5}$ ),

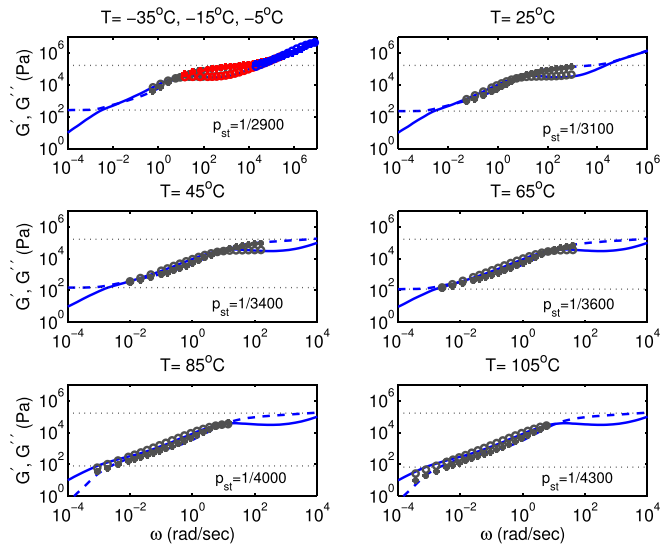


**FIG. 7.** Comparison between experimental (symbols) and theoretical storage and loss moduli (dashed and solid lines, respectively) of sample PnBA-AA13, at several temperatures. The best fit value of  $p_{st}$  is also shown. Dotted lines show  $G_{N,tot}^0$  and  $G_{N,trapped}^0$ .

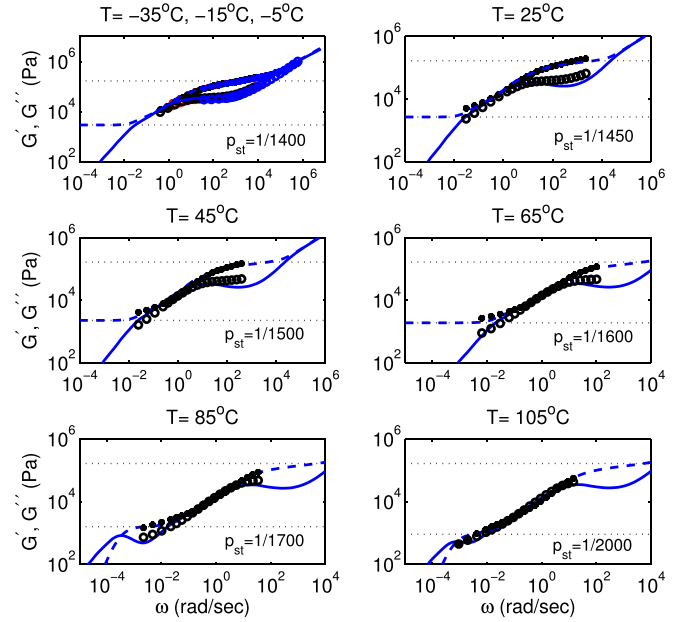


**FIG. 8.** Comparison between experimental (symbols) and theoretical storage and loss moduli (dashed and solid lines, respectively) of sample PnBA-AA38, at several temperatures. The best fit value of  $p_{st}$  is also shown. Dotted lines show  $G_{N,tot}^0$  and  $G_{N,trapped}^0$ .

and  $B = -120^\circ\text{C}$  ( $-47^\circ\text{C}$ ) for PnBA-AA13 (PnBA-AA38). Figure 9 also shows that, for a given temperature,  $p_{st}$  rises with increasing AA content. Since  $p_{st}$ , the probability of a monomer to act as a sticky junction, decays with temperature, the level of the second plateau,  $G_{N,trapped}^0$ , also reduces with decreasing temperature (see also Fig. 10 below).

It can be seen from Figs. 7 and 8 that for the highest two temperatures and for both materials the assumption of an infinite lifetime is too strong. Therefore, a finite association lifetime for the sticky junctions must be considered in order to capture the onset of the terminal regime. For the PnBA-AA13 copolymer, the following values have been used:  $\tau_{ass} = 3 \times 10^2 \text{ s}$  at both  $85^\circ\text{C}$  and  $105^\circ\text{C}$ . Here, the CRR equilibration time,  $\tau_{CR,R}$ , is longer than  $\tau_{ass}$ ; that is,  $\tau_{CR,R}$  is  $\approx 1500 \text{ s}$  and so in the model both faster CRR modes and

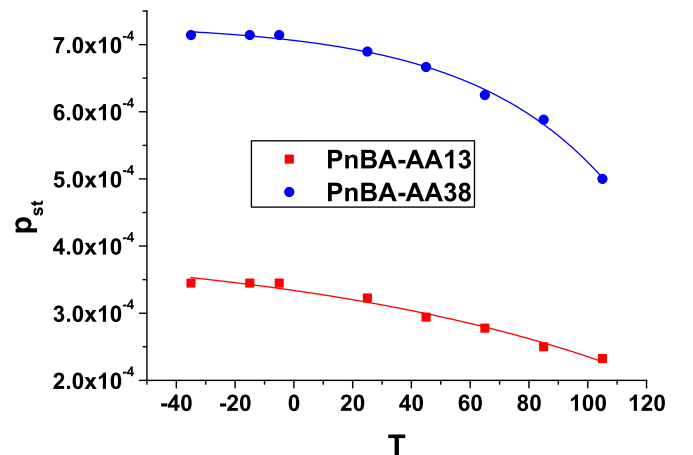


**FIG. 9.**  $p_{st}$  vs temperature for PnBA-AA13 and PnBA-AA38 (squares and circles, respectively). The lines correspond to single exponential decays.

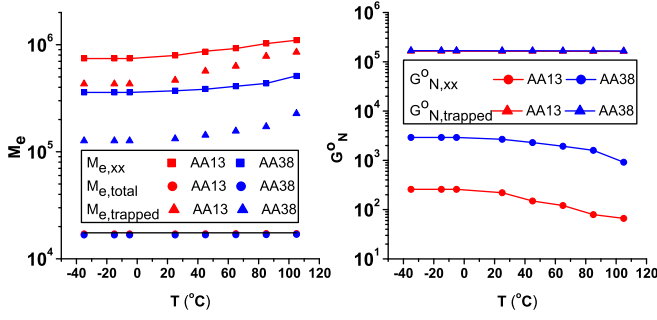


FIG. 10. Left: Evolution of  $M_{e,total}$ ,  $M_{e,trapped}$ , and  $M_{e,xx}$  as a function of temperature for PnBA-AA13 and PnBA-AA38. Lines are the predictions of Eq. (19). The horizontal line corresponds to  $M_{e,ent}$ . Right: The corresponding  $G_{N,total}^0$  and  $G_{N,trapped}^0$ .

aggregate dissociation contribute to the terminal relaxation. For the PnBA-AA38 sample, the data are fitted using  $\tau_{ass} = 6 \times 10^3$  s and  $\tau_{ass} = 3 \times 10^3$  s at 85 °C and 105 °C, respectively. Here,  $\tau_{CR,R}$  is considerably shorter than  $\tau_{ass}$  at both temperatures therefore the terminal relaxation is controlled by the dissociation of aggregates. All values of  $\tau_{ass}$  are more than two orders of magnitude larger compared to  $\tau_{obs}$ . Nevertheless, we do not wish to attach heavy significance to them since terminal flow is not completely reached in the experimental frequency window, a fact that does not allow us to discuss the temperature effect on the terminal relaxation time.

As explained in Sec. III B 3,  $p_{st}$  is the only fit parameter. All the other parameters are calculated from this value. For each temperature, the corresponding molecular characteristics of the mobile and immobile (trapped) components of PnBA-AA13 and PnBA-AA38 copolymers are shown in Tables II and III, respectively. Using (i) the volume fractions presented in these tables, (ii) the estimated value of  $M_{e,xx}$ , (iii) the expression  $M_{e,trapped} (= M_{e,total}/\nu_t^2)$  as well as (iv) Eqs. (10) and (16), we have obtained the temperature evolution of  $M_{e,trapped}$  and  $M_{e,total}$ , presented in the left panel of Fig. 10 together with  $M_{e,xx}$ . We have also obtained the temperature evolution of  $G_{N,trapped}^0$  and  $G_{N,total}^0$  that is shown in the right panel of Fig. 10. From Fig. 10, and Tables II and III, we conclude that the proportion of trapped strands is quite low, i.e., 2%–4% and 7%–13% for PnBA-AA13 and PnBA-AA38, respectively. In consequence, the difference in the level of the (total) plateau modulus,  $G_{N,total}^0$ , of the two copolymers is negligible, which is consistent with the observation made on the experimental data. Also, we observe that the average molecular weight between two stickers is large ranging from 360 k to 510 k and 746 k to 1100 k, for samples PnBA-AA13 and PnBA-AA38, respectively. In both cases,  $M_{e,xx}$  exceeds the molecular weight of the copolymer itself. Moreover, for all examined temperatures, it is larger for PnBA-AA13 than for PnBA-AA38 since in the latter case  $p_{st}$  is larger and thus the volume fraction of free chains is lower. Moreover, for a given sample, it is larger than  $M_{e,trapped}$  since it does not account for frozen entanglements. Note that the estimated values of  $M_{e,xx}$  follow the Flory equation [That is, Eq. (19) cf. red and blue lines at the left panel of Fig. 10].

The reason for which  $M_{e,xx}$  exceeds 210 k, the molecular weight of the copolymer, is explained as follows.  $M_{e,xx}$  is

determined by looking at the molecular weight between long lifetime stickers of an “infinitely” long chain. That is, in the statistical approach described in Sec. III B 3 polymer portions of  $M_w = 210$  k are not classified into different chains according to the number of long lifetime stickers they contain, but they are treated as molecular segments of one, extremely long polymer chain. Obviously, the molecular weight between long lifetime stickers has a distribution (polydispersity);  $M_{e,xx}$  corresponds to the average molecular weight of this distribution. Since the used values of  $p_{st}$  lead to large fractions of free chains and starlike molecules, at the corresponding “infinite” chain many polymer portions between long lifetime stickers have molecular weight that exceeds the molecular weight of the copolymer itself. As a result,  $M_{e,xx}$  is larger than 210 k.

In terms of molecular relaxation, our simulations indicate that most chains simply relax by reptation and/or CLF. For example, Fig. 11 presents the storage modulus of the PnBA-AA13 copolymer (black solid line) at  $T = 45$  °C together with the contribution of each component, i.e., the free linear chains, the starlike chains, and the dangling arms of the trapped chains (see label). The storage modulus of the reference material is also shown for comparison. Here,  $\nu_f = 0.61$ ,  $\nu_s = 0.30$ ,  $\nu_d = 0.06$ , and  $\nu_t = 0.03$ . We note a small shift toward lower frequencies of the terminal cross-over of the linear chains in the PnBA-AA13 sample as compared to the respective cross over of the reference material. This behavior is explained as follows. For the molecular weight of 210 kg/mol, corresponding to  $\approx 10$  entanglement segments, the reptation time (when  $\Phi_{active}(t) = 1$ , as it is the case here) is similar to the terminal CLF fluctuation time of the half arm (molecular weight of 105 kg/mol). Since we consider that  $\Phi_{active}(t) = 1$  the reptation process of the free chains is not affected by the presence of sticky junctions in

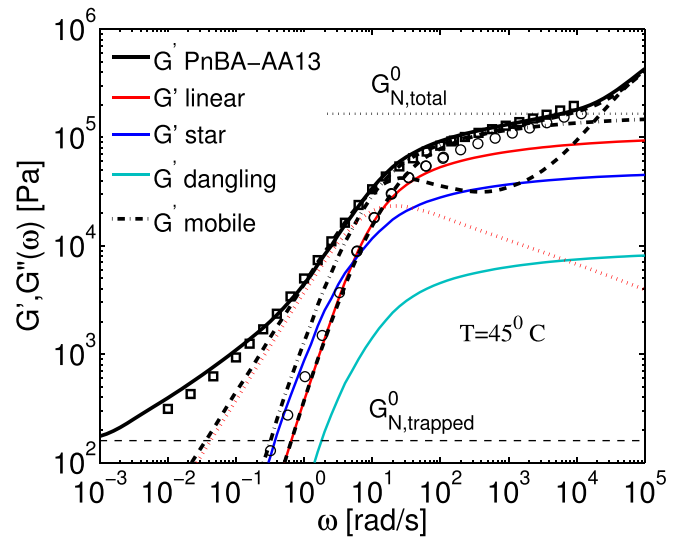


FIG. 11. Theoretical (black solid line) and experimental (squares)  $G'$ , of the PnBA-AA13 copolymer at  $T = 45$  °C. The storage modulus of each component is also shown as well as  $G'$  and  $G''$  of the reference material at the same temperature (dashed lines).  $G'$  mobile (dashed-dotted line) is the sum of all three mobile components (linear, star, and dangling). Circles correspond to  $G'$  data of the reference material. The dotted line is the  $G''$  of the linear chains.

the surrounding environment. Nevertheless, we observe that the retraction process of the arms of the free chains is delayed due to the trapped chains and the unrelaxed sections of their dangling arms; this process is also delayed due to the unrelaxed portions of the starlike chains [see Eq. (14); for the linear chains in the reference PnBA, i.e., in the absence of stickers, one should consider  $\Phi(\xi) = 1 - \xi$ ]. The orange line in Fig. 11 ( $G'$  mobile) corresponds to the sum of the storage modulus of all three mobile components. (The Rouse contribution is neglected in the calculation of  $G'$  of the mobile fraction.) Up to  $\omega \approx 10$  rad/s, this curve follows closely the storage modulus of the copolymer. Then all mobile fraction fully relaxes and relaxation of the copolymer continues with CRR equilibration of the trapped strands.

Overall, the model proposed in this article appears to be useful for the description of linear dynamic viscoelasticity data of supramolecular networks that have the following characteristics: (i) Consist of entangled associating chains that carry a small number of long lifetime stickers and (ii) constitute of binary associations which their lifetime is much faster compared to rheological chain relaxation. Owing to the small number of long lifetime associations, these systems typically manifest a second low frequency plateau, and have a high fraction of mobile material, i.e., chains or chain strands that can normally relax by reptation and/or CLFs. Thus, the present model is suitable for systems such as the PnBA-AA38 copolymer presented herein, and the sulfonated ionomers of [37]. There, the relaxation following the upper plateau was identified with relaxation of the “end sections” of the chains, that is, the portions of the chain lying between the free chain ends and the ionic aggregates closest to each chain end. Nevertheless, a quantitative analysis of the data was impeded by the lack of suitable model; it would be interesting to examine whether our model can quantitatively describe these data. On the other hand, the low frequency data in Fig. 7 (PnBA-13AA) demonstrate a shoulder rather than a second plateau. It is possible that other relaxation modes, like hindered reptation, or combination of those modes with CRR, control the intermediate and terminal response of the material. Despite the success in fitting the data, it might be the case that application of the present model is not appropriate for the PnBA-13AA sample, owing to the too small fraction of trapped strands; this might explain the unrealistic values that some parameters take in this case, e.g.,  $N_{ent}$  ranges, in average, from 24 to 49. (The range of values of  $N_{ent}$ , the number of entanglements between sticky junctions or/and frozen entanglements, is more realistic in the case of PnBA-38AA; there  $N_{ent}$  ranges from 7 to 11.)

## V. CONCLUSIONS

In this work, we propose a candidate explanation for two surprising features observed in small amplitude oscillatory shear (SAOS) experiments on two associating PnBA-AA copolymers: (i) The emergence of a second, low frequency, plateau in  $G'$  (clearly evident for PnBA-AA38, but not for PnBA-AA13), the level of which depends on temperature

and density of AA groups, and (ii) the parallel decay of  $G'$  and  $G''$  at intermediate frequencies prior to the aforementioned second plateau zone. We attributed these two features to the presence of long lifetime stickers (aggregates/sticky junctions). Single hydrogen bonding (AA dimmers) was completely neglected in this study. In an accompanying work [35], the opposite physical picture is examined, that is, the attention is drawn to the effects of single hydrogen bonding on the dynamics, and long lifetime stickers are omitted. By incorporating the idea of sticky junctions into the TMA, we have shown that the rheological measurements are reasonably captured by the present model. Within our theoretical framework, the low frequency plateau zone arises from unrelaxed chain orientation at large length scales while feature (ii) above is due to CRR equilibration of trapped stands (chain portions between adjacent sticky junctions or/and trapped entanglements) following the relaxation of the mobile polymer chains, which have at least one end not attached to sticky junctions. The fact that the model well captures the dynamics of the PnBA-AA38 sample at intermediate frequencies indicates that CRR is indeed a candidate molecular level explanation of the observed behavior. The molecular characteristics of the mobile and trapped portions were determined using a statistical approach at the cost of one additional parameter only. Finally, we note that thermorheological complexity was observed for both PnBA-AA copolymers.

## ACKNOWLEDGMENTS

The authors are grateful to C. A. Fustin, J. Brassinne, F. Zhuge, and E. Simonini for helpful discussions. This work was financially supported by the European Union through the “SUPOLEN” Marie Curie 7th Framework Initial Training network. E.v.R. and H.G. thank FNRS for financial support.

## References

- [1] Semenov, A. N., and M. Rubinstein, “Dynamics of entangled associating polymers with large aggregates,” *Macromolecules* **35**, 4821–4837 (2002).
- [2] van Ruymbeke, E., D. Vlassopoulos, M. Mierzwa, T. Paluka, D. Charalabidis, M. Pitsikalis, and N. Hadjichristidis, “Rheology and structure of entangled telechelic linear and star polyisoprene melts,” *Macromolecules* **43**, 4401–4411 (2010).
- [3] Brassinne, J., A. M. Stevens, E. van Ruymbeke, J. F. Gohy, and C. A. Fustin, “Hydrogels with dual relaxation and two-step gel-sol transition from heterotelechelic polymers,” *Macromolecules* **46**, 9134–9143 (2013).
- [4] Wietor, J. L., D. J. M. van Beek, G. W. Peters, E. Mendes, and R. P. Sijbesma, “Effects of branching and crystallization on rheology of polycaprolactone supramolecular polymers with ureidopyrimidinone end groups,” *Macromolecules* **44**, 1211–1219 (2011).
- [5] Lewis, C. L., K. Stewart, and M. Anthamatten, “The influence of hydrogen bonding side-groups on viscoelastic behavior of linear and network polymers,” *Macromolecules* **47**, 729–740 (2014).
- [6] Chen, Q., G. J. Tudryn, and R. H. Colby, “Ionomer dynamics and the sticky Rouse model,” *J. Rheol.* **57**, 1441–1462 (2013).

- [7] Chen, Q., H. Masser, H. S. Shiau, S. Liang, J. Runt, P. C. Painter, and R. H. Colby, "Linear viscoelasticity and Fourier transform infrared spectroscopy of polyetherestersulfonate copolymer ionomers," *Macromolecules* **47**, 3635–3644 (2014).
- [8] Brassinne, J., C. A. Fustin, and J. F. Gohy, "Polymer gels constructed through metalligand coordination," *J. Inorg. Organomet. Polym. Mater.* **23**, 24–40 (2013).
- [9] Doi, M., and S. F. Edwards, *The Theory of Polymer Dynamics* (Clarendon, Oxford, 1986).
- [10] McLeish, T. C. B., "Tube theory of entangled polymer dynamics," *Adv. Phys.* **51**, 1379–1527 (2002).
- [11] Marrucci, G., "Relaxation by reptation and tube enlargement: A model for polydisperse polymers," *J. Polym. Sci.* **23**, 159–177 (1985).
- [12] Likhtman, A. E., and T. C. B. McLeish, "Quantitative theory for linear dynamics of linear entangled polymers," *Macromolecules* **35**, 6332–6343 (2002).
- [13] Glomann, T., G. J. Schneider, A. R. Brás, W. Pyckhout-Hintzen, A. Wischniewski, R. Zorn, J. Allgaier, and D. Richter, "Unified description of the viscoelastic and dielectric global chain motion in terms of the tube theory," *Macromolecules* **44**, 7430–7437 (2011).
- [14] Matsumiya, Y., K. Kumazawa, M. Nagao, O. Urakawa, and H. Watanabe, "Dielectric relaxation of monodisperse linear polyisoprene: Contribution of constraint release," *Macromolecules* **46**, 6067–6080 (2013).
- [15] Read, D. J., K. Jagannathan, S. K. Sukumaran, and D. Auhl, "A full-chain constitutive model for bidisperse blends of linear polymers," *J. Rheol.* **56**, 823–873 (2012).
- [16] Watanabe, H., T. Sawada, and Y. Matsumiya, "Constraint release in star/star blends and partial tube dilation in monodisperse star systems," *Macromolecules* **39**, 2553–2561 (2006).
- [17] Shivokhin, M. E., E. van Ruymbeke, C. Bailly, D. Kouloumasis, N. Hadjichristidis, and A. E. Likhtman, "Understanding constraint release in star/linear polymer blends," *Macromolecules* **47**, 2451–2463 (2014).
- [18] van Ruymbeke, E., V. Shchetnikava, Y. Matsumiya, and H. Watanabe, "Dynamic dilution effect in binary blends of linear polymers with well-separated molecular weights," *Macromolecules* **47**, 7653–7665 (2014).
- [19] Baxandall, L. G., "Dynamics of reversibly cross-linked chains," *Macromolecules* **22**, 1982–1988 (1989).
- [20] Leibler, L., M. Rubinstein, and R. H. Colby, "Dynamics of reversible networks," *Macromolecules* **24**, 4701–4707 (1991).
- [21] Shabbir, A., S. Goldansaz, O. Hassager, E. van Ruymbeke, and N. J. Alvarez, "The effect of hydrogen bonding on linear and nonlinear rheology of entangled polymer melts," *Macromolecules* **48**, 5988–5996 (2015).
- [22] Goldansaz, H., C. A. Fustin, M. Wübbenhorst, and E. van Ruymbeke, "How Supramolecular Assemblies Control Dynamics of Associative Polymers: Toward a General Picture," *Macromolecules* (2016). [E-pub ahead of print].
- [23] Nyrkova, I. A., A. R. Khokhlov, and M. Doi, "Microdomain structures in polyelectrolyte systems: Calculation of the phase diagrams by direct minimization of the free energy," *Macromolecules* **27**, 4220–4230 (1994).
- [24] van Ruymbeke, E., R. Keunings, and C. Bailly, "Prediction of linear viscoelastic properties for polydisperse mixtures of entangled star and linear polymers: Modified tube-based model and comparison with experimental results," *J. Non-Newtonian Fluid Mech.* **128**, 7–22 (2005).
- [25] Ahmadi, M., C. Bailly, R. Keunings, M. Nekoomanesh, H. Arabi, and E. van Ruymbeke, "Time marching algorithm for predicting the linear rheology of monodisperse comb polymer melts," *Macromolecules* **44**, 647–659 (2011).
- [26] Shchetnikava, V., J. J. M. Slot, and E. van Ruymbeke, "A comparison of tube model predictions of the linear viscoelastic behavior of symmetric star polymer melts," *Macromolecules* **47**, 3350–3361 (2014).
- [27] Milner, S. T., and T. C. B. McLeish, "Reptation and contour-length fluctuations in melts of linear polymers," *Phys. Rev. Lett.* **81**, 725–728 (1998).
- [28] Dong, J., Y. Ozaki, and K. Nakashima, "Infrared, Raman, and near-infrared spectroscopic evidence for the coexistence of various hydrogen-bond forms in poly(acrylic acid)," *Macromolecules* **30**, 1111–1117 (1997).
- [29] Blottière, B., T. C. B. McLeish, A. Hakiki, R. N. Young, and S. T. Milner, "Rheology and tube model theory of bimodal blends of star polymer melts," *Macromolecules* **31**, 9295–9304 (1998).
- [30] Milner, S. T., T. C. B. McLeish, R. N. Young, A. Hakiki, and J. M. Johnson, "Dynamic dilution, constraint-release, and star-linear blends," *Macromolecules* **31**, 9345–9353 (1998).
- [31] van Ruymbeke, E., Y. Masubuchi, and H. Watanabe, "Effective value of the dynamic dilution exponent in bidisperse linear polymers: From 1 to 4/3," *Macromolecules* **45**, 2085–2098 (2012).
- [32] Colby, R. H., X. Zheng, M. H. Rafailovich, J. Sokolov, D. G. Peiffer, S. A. Schwarz, Y. Strzhemechny, and D. Nguyen, "Dynamics of lightly sulfonated polystyrene ionomers," *Phys. Rev. Lett.* **81**, 3876–3879 (1998).
- [33] Tierney, N. K., and R. A. Register, "Ion hopping in ethylene-methacrylic acid ionomer melts as probed by rheometry and cation diffusion measurements," *Macromolecules* **35**, 2358–2364 (2002).
- [34] Stadler, F. J., W. Pyckhout-Hintzen, J. M. Schumers, C. A. Fustin, J. F. Gohy, and C. Bailly, "Linear viscoelastic rheology of moderately entangled telechelic polybutadiene temporary networks," *Macromolecules* **42**, 6181–6192 (2009).
- [35] Ahmadi, M., L. G. D. Hawke, H. Goldansaz, and E. van Ruymbeke, "Dynamics of entangled linear supramolecular chains with sticky side groups: Towards inclusion of hindered fluctuations," *Macromolecules* **48**, 7300–7310 (2015).
- [36] Zosel, A., and G. Ley, "Influence of crosslinking on structure, mechanical properties, and strength of latex films," *Macromolecules* **26**, 2222–2227 (1993).
- [37] Tierney, N. K., and R. A. Register, "Synthesis and melt dynamics of model sulfonated ionomers," *Macromolecules* **36**, 1170–1177 (2003).